

# Electrochemical detection of structurally different aminoacids by thin layers of undoped and doped ZnO

Pavel Dytrych, Petr Kluson, Petr Stanovsky, Olga Solcova

Institute of Chemical Process Fundamentals, v.v.i.

The Czech Academy of Sciences

Rozvojova 135, 16502 Prague 6, Czech Republic

[dytrych@icpf.cas.cz](mailto:dytrych@icpf.cas.cz)

**Abstract**—Thin layers of undoped and doped ZnO were prepared by a sol-gel method using the dip-coating technique. The doped layers contained 10 mol. % of Li or 10 mol. % of Na. The films were yielded with thicknesses ranging from 140 nm to 160 nm. The layers were analyzed by SEM, EDX, XRD, Raman spectroscopy, and by electrochemical tests (amperometry, linear voltammetry, and open circuit potential). All prepared samples were smooth and transparent. A series of electrochemical measurement was performed with both doped and undoped layers with aminoacids solutions of electrolyte. The glycine, glutamic acid, histidine, and methionine were chosen. Glycine possesses alkane chain, glutamic acid the second carboxylic group, histidine the alkalic amino group, and methionine the sulphur containing group. It was shown, that the change in polarity of ZnO induced by doping with 10 mol. % Na and 10 mol. % Li played an important role in surface interaction of ZnO and aminoacid dissolved in the electrolyte and permitted the qualitative and semi-quantitative distinguishing of the four structurally different aminoacids.

**Keywords**— *doped semiconductors; ZnO; aminoacids, open circuit amperometry;*

## I. INTRODUCTION

ZnO belongs to the group of semiconductors based on metal oxides, which are useful for UV and visible light-emitting electrochemical devices due to its wide band-gap ( $\approx 3.3$  eV at ambient temperature) and other optical and electronic properties [1-4]. These properties depend on the type and amount of impurities, dopants, concentration of defects, crystallinity, surface morphology, etc. [5-7]. A special interest was given to the field of inter-facial behavior and sensorics [7], where the thin films of zinc oxides play an important role in many detection systems [8, 9]. A variety of techniques have been utilized in the past to produce zinc oxide thin films. Sputter deposition techniques [10-13], chemical vapor deposition [14, 15], liquid phase deposition [16-18], electrochemical deposition [19-21], and spray pyrolysis [22] are among the most prominent methods. Recently it was shown, that the modification of ZnO surfaces by

bio-reactive amino groups (e.g. aminopropyl triethoxysilane) led to specific interaction of ZnO layers with peptides [23-25]. Zinc oxides layers' affinities to polar molecules can be also enhanced by dopation with polar dopants (e. g. Li, Na) [24-27]. The affinity of the ZnO surface to the aminoacids  $-\text{COOH}$ ,  $-\text{NH}_2$  groups could also be enhanced by another structural modification. On the other hand, the right choice of the aminoacids could also improve their detection by modified ZnO surfaces [25]. In this communication we report on electrochemical properties of doped and undoped ZnO films produced by sol-gel method using dip-coating technique and their application as viable sensors for four types of structurally different aminoacids in the electrolyte, namely alkane chain containing glycine, highly polar glutamic acid, alkalic histidine and sulphur containing methionine. The intentional change in polarity caused by doping with Li or Na could lead to specific interaction of ZnO surface with the electrolyte containing polar aminoacids.

## II. EXPERIMENTAL

Thin layers of ZnO were prepared by sol-gel method and dip-coating technique. The ZnO films via sol-gel were prepared by mixing propan-2-ol (Sigma Aldrich, Germany), zinc acetate dihydrate (Sigma Aldrich, Germany) and diethanolamine (DEA) (Sigma Aldrich, Germany). The molar ratio between  $\text{Zn}^{2+}$  and DEA was kept 1:1, the concentration of  $\text{Zn}^{2+}$  was set at  $0.45 \text{ mol L}^{-1}$  in propan-2-ol. In the case of doped layers, LiOH (Sigma Aldrich, Germany),  $\text{KNO}_3$  (Sigma Aldrich, Germany) were added to the solution in the form of powder and dissolved for 30 min. The layers were prepared with 10 molar % of Li, Na vs.  $\text{Zn}^{2+}$  ( $0.045 \text{ mol L}^{-1}$ ). As substrates ITO (Indium Tin Oxide) glass slides ( $20 \times 12.5 \times 1.1 \text{ mm}$ ,  $15\text{-}20 \ \Omega \text{ cm}$ , Delta Technologies, USA) were chosen. The substrate was held using a movable substrate holder (vertically) in a position above the solution of sol-gel. The next step was a linear movement with the speed of  $1.5 \text{ mm s}^{-1}$  into the sol container. The substrate was kept in the solution for 30 s. Thereafter the movable substrate holder moved upwards with a linear speed of  $1 \text{ mm s}^{-1}$ . The formation of a thin sol layer was observed during this movement. This technique produces layers deposited on both sides of the substrate, therefore one side was wiped off by cellulose and layers were air-

dried. Air-drying was performed at 110 °C for 30 minutes with subsequent calcination at 500 °C for 5 h.

For a detailed physical behavior of the prepared layers a series of characterization methods was used. The crystallographic structure was determined from Raman spectroscopy (Nicolet Almega XR) and from X-ray diffraction analyses (Pananalytical - MRC with Cu anode). The angle of incident X-rays was set to 0.5°. The crystalline size was obtained using a method developed from X-ray diffraction data by Pawley as used in TOPAS software [23]. SEM images were obtained at Tescan Indusem with Quantax 200 and XFlash detector 5010, Bruker. Thicknesses were determined by cross-section photos taken by SEM (angle 85-87°). XPS spectra were obtained by Kratos Amicus/ESCA 3400 with working pressure lower than  $5.0 \cdot 10^{-7}$  Pa, using polychromatic Mg X-Ray source (Mg K $\alpha$ , 1253.4 eV). Spectra were taken over Zn 2p, O 1s, C 1s, Na 1s, Li 1s. Samples were sputtered with Ar<sup>+</sup> ions at 500 V with current of 10 mA for 30 s. The overlapping spectral features were resolved into individual components using the damped non-linear least squares method and the lines of Gaussian-Lorentzian shape. Prior to fitting the Shirley background was subtracted [28].

All measurements were performed using an optical-bench set-up [16]. The system consists of a medium-pressure mercury lamp (Arc Lamp, LOT-Oriel, 500 W), which emits polychromatic light followed by optical filters, shutter and an electrochemical cell connected to the potentiostat. A 0.1 mol L<sup>-1</sup> solution of Na<sub>2</sub>SO<sub>4</sub> acts as electrolyte. The potential inserted to the cell was operated by a computer-controlled potentiostat Voltalab 10 PGZ-100. Data were acquired and analyzed in Volta Master 4 (v. 7.08). Standard electrochemical methods were used, namely: open circuit potential (OCP), cyclic voltammetry (CV), linear voltammetry (LV), and amperometry (AMP). The time dependence of potential of electrode/electrolyte interface was measured using OCP for undoped and doped layers in a classical three electrode system [16]. The computer-controlled shutter was closed at the beginning of the irradiation experiment and opened after 30 s. The light then passed through the shutter and irradiated the sample. The interval between two points was set to 0.1 or 0.2 s to see the rapid change of potential after irradiation. The shutter was opened for next 60 s.

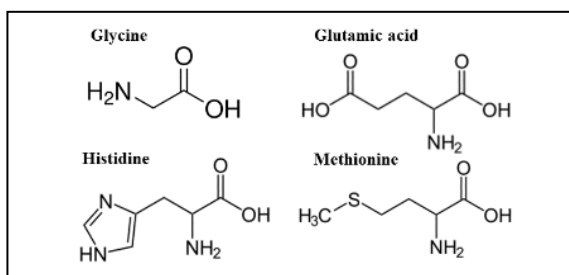


Fig. 1: Chemical structures of tested aminoacids

The measurement continued in dark for 60 s. The structures of aminoacids are shown in Fig. 1. Glycine, glutamic acid, histidine and methionine in a form of powder with p.a. purity (Sigma Aldrich, Germany) were separately added as studied species to the standard 0.1 mol L<sup>-1</sup> Na<sub>2</sub>SO<sub>4</sub> (see Tab.1) electrolyte during measurement of ZnO (photo)-electrochemical properties of the processes occurring on ZnO/electrolyte - aminoacid interface. The concentration of individual aminoacids` storage solutions was set to  $1 \cdot 10^{-3}$  mol L<sup>-1</sup> of electrolyte. Individual aminoacids mixture was then added to the electrochemical cell using the automatic pipette by 0.5 ml or 1 ml steps. The formed solution in the electrochemical cell was stirred for 15 s to allow homogenization of the modified electrolyte. After every addition only two electrochemical measurements were performed with the aminoacid solution (OCP and CV). The OCP started at -200 mV vs. the standard

TABLE 1: BASIC PHYSICO-CHEMICAL PROPERTIES OF STUDIED AMINOACIDS

Aminoacid	pl	pKa – carboxyl group	pKa – amino group
Glycine	6.01	2.34	9.6
Glutamic acid	3.15	2.1	9.47
Histidine	7.6	2.13	9.28
Methionine	5.74	1.8	9.33

Ag/AgCl(s) electrode. The following CV was performed from -0.2 to 1.2 V with return to - 200 mV with the linear change of potential of 50 mV s<sup>-1</sup> for 3 times. When 9 ml of the aminoacids solution were stepwise added to the main electrolyte both measurements (OCP and CV) were performed.

### III. RESULTS AND DISCUSSION

#### A. Characterization of layers

All layers of ZnO were crystalline and revealed no specific preferential growth direction as can be seen in Fig. 2. The unindexed peaks were obtained from ITO glass substrate. In Fig. 2 the small changes of diffraction angles can be attributed to the implantation of dopant atoms to the ZnO structure. This can be ascribed to the preparation route, in which the dopants are directly added to the maternal solution of Zn<sup>2+</sup> causing only very small changes to the solution. This leads to the formation of similarly structured crystallites of undoped and doped ZnO. The size of crystallites was calculated by Pawley based method in the TOPAS software [28] and the results are summarized in Tab. 2

TAB. 2: CRYSTALLITE SIZE OF ZNO

Sample	Crystallite size [nm]
ZnO	59 ± 3
ZnO 10 mol. % Na	61 ± 3
ZnO 10 mol. % La	62 ± 3

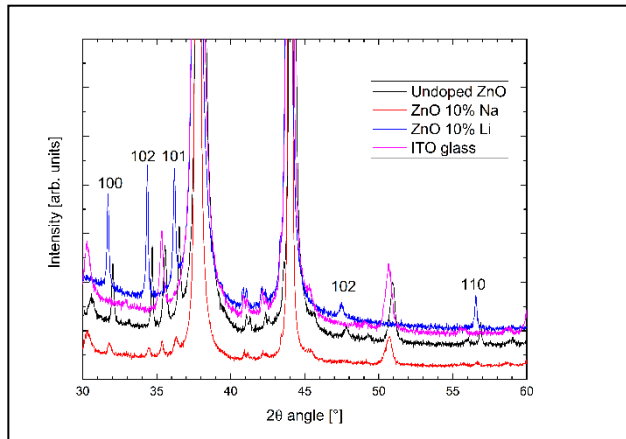


Fig. 2: XRD diffractograms of ZnO layers deposited on ITO glass

Obtained results corroborate that the doping had almost no effect on the calculated crystallite size which was approximately 60 nm for all ZnO samples. Despite the carbon containing species used in the preparation of layers, only minor traces of carbon were observed in the whole range of Raman spectrum. All characteristic peaks were found for ZnO (Fig. 3) showing the formation of wurtzite type of ZnO for all three types of layers. Only small changes between the undoped and doped layers by means of Raman spectroscopy were observed. As can be seen in Fig. 4a, only  $Zn^{2+}$  (2p 1/2 at 1022.5 eV, 2p 3/2 at 1046.1 eV) oxidation states were obtained for all layers, despite the high doping level of the dopants. In Fig. 4b the broadening of O 1s can be attributed to a mixture of Zn – O [29, 30], Li – O [29, 30], as well as adsorbed species (water and –OH groups) [29]. The appearance of these peaks verifies the changed polarity of the ZnO surfaces caused by doping.

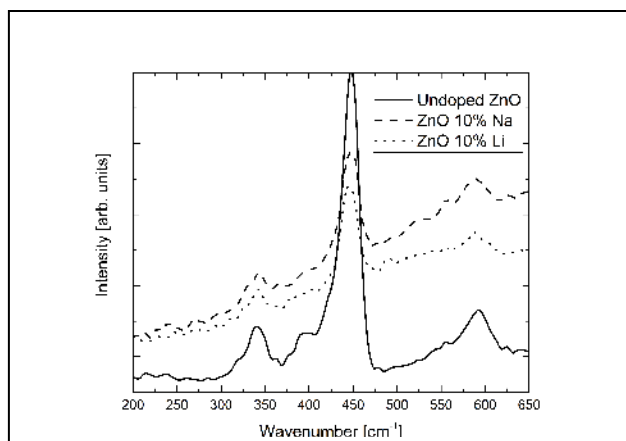


Fig. 3: Comparison of Raman spectra obtained for undoped and doped layers

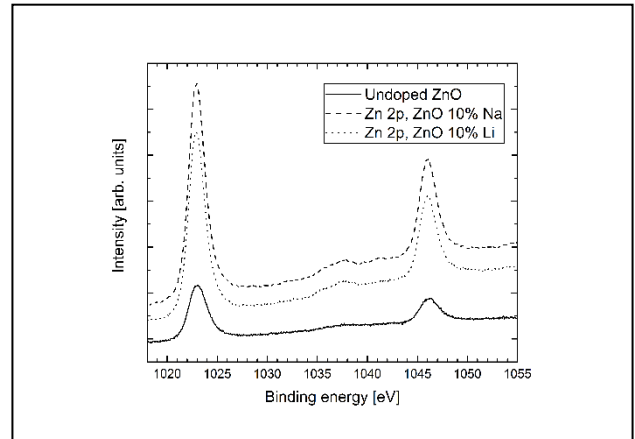


Fig 4a: XPS spectra of O 1s

This Fig. 4 also proves the occurrence of Zn-O-Li [29], resp. Zn-O-Na [30] bonds. It was found, that the C 1s signal from the measured samples comes from the adsorbed species on the surfaces. The amount of carbon after sputtering with Ar (1 kV, 10 mA, and 1 min) dramatically decreased. The final amount of carbon was below 1 mol. %. The stoichiometry at the clean surface can be summarized as  $Zn(0.95-1.0)O(0.95-1.1)$ ,  $Zn(0.95-1.02)Li(0.08-0.11)O(1.04-1.06)$  and  $Zn(0.96-1.03)Na(0.08-0.13)O(1.04-1.05)$ . The chemical composition of Li doped layer after two amperometry measurements showed the partial exchange of Li for Na and almost full disappearance of Li forming  $Zn(0.95-1.02)O(1.04-1.05)Na(0.01-0.02)$ .

#### B. Photo-electrochemistry of undoped and doped ZnO

Values of generated photocurrents for both types of undoped layers as well for doped layer were measured at constant potential (0.6 V against the standard Ag/AgCl electrode) by amperometry. The obtained curves indicated the photocurrent-time behavior of the layers. The lowest photocurrent densities were observed for undoped ZnO layers. The Na doped layers showed a little bit higher response to the incident light than undoped layers. The highest current densities

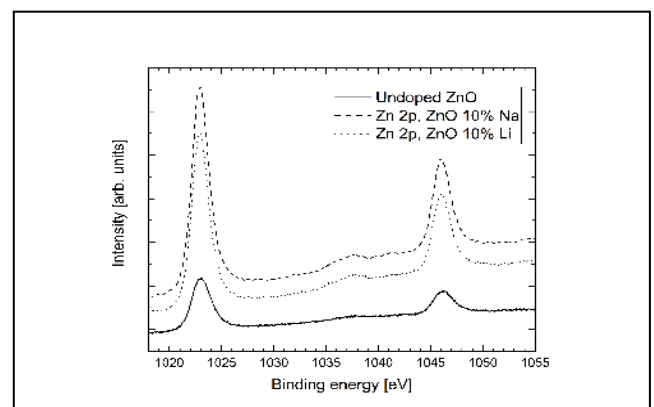
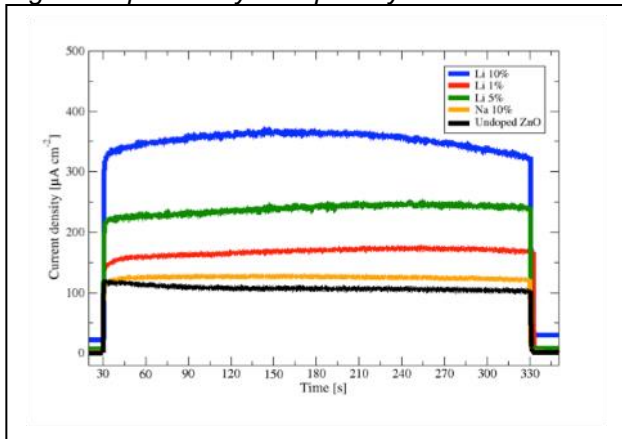


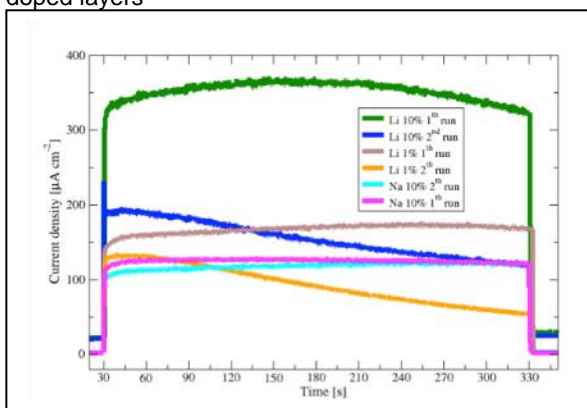
Fig 4b: XPS spectra of Zn 2p

Fig. 5: Amperometry of doped layers of ZnO



were obtained for Li doped layers, where the current densities were a function of Li incorporated to the structure. This means that the Li was emitted to the electrolyte and enhanced the conductivity or increased the generation of electrons and holes in the ZnO matrix. It can be easily seen for the highest content of Li (Fig. 5), where after the half of the irradiation period the current density sank rapidly. As a confirmation of this idea a second run of amperometry was performed under same operation conditions. The resulted dependence can be seen in Fig. 6, where the current densities of Li doped layers decreased exponentially. On the other hand, for thin layers of Na doped ZnO no significant changes were found. This is caused by the semiconductor-electrolyte interface, where a huge concentration of Na from electrolyte acts against the dissolution of Na doped layers. The stability if dopants in the layers depends on the dissolution kinetics to the electrolyte. In the case of Na dopant, there is a  $0.1 \text{ mol L}^{-1}$  solution of  $\text{Na}_2\text{SO}_4$  acting against the dissociation of Na from the layer. In the case of Li, the change of the chemical potential on both sides of the interface cause the dissolution of Li to the electrolyte. The dissolution of Li to the electrolyte was confirmed by XPS.

Fig. 6: Comparison of 1<sup>th</sup> and 2<sup>nd</sup> runs of amperometry for doped layers



C. Electrochemical detection of aminoacids on undoped ZnO layers

A series of OCP measurements was done for undoped and doped layers of ZnO with the aminoacids solution of electrolyte. The aminoacids for the experiment were chosen based on their polarities and the isoelectric point value (pI) owing to that the aminoacids reveal distinct polarities and acidity (basicity) as a function of their structure [31]. Tab. 1 shows the electrochemical properties of used aminoacids. Glycine represents the alkane group containing specie, the glutamic acid possesses the highest acidity and histidine was chosen due to its alkalic behavior. The glycine molecule (isoelectric point value pI = 6.06) is the “smallest” one among other tested aminoacids, thus the reaction could reveal the interaction of glycine with the differently polar surfaces of undoped/doped ZnO [30]. The Fig. 7a represents the concentration and OCP dependence on time. As can be clearly seen even small changes between the standard  $0.1 \text{ mol L}^{-1} \text{ Na}_2\text{SO}_4$  solution and the  $2.44 \cdot 10^{-5} \text{ mol L}^{-1}$  solution resulted in a very distinct OCP time evolution. This is caused by the strong reaction of glycine on the surface of ZnO resulting in change of adsorption of other species (electrolyte). This OCP and concentration on time dependence proves the polar behavior of the ZnO, which surface strongly interacts with polar molecules in the electrolyte [24-26].

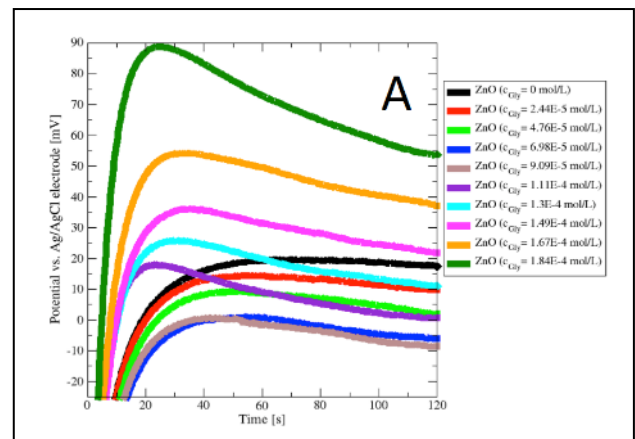


Fig. 7a: OCP measurement for on undoped ZnO layer with glycine

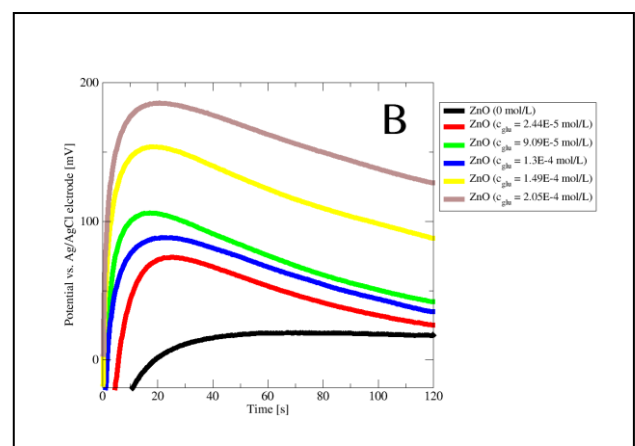


Fig. 7b: OCP measurement for on undoped ZnO layer with glutamic acid

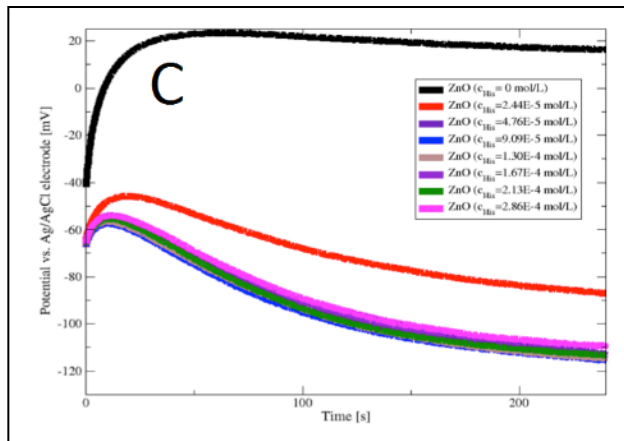


Fig. 7c: OCP measurement for on undoped ZnO layer with histidine

It generally leads to the change of the number of charged species on the semiconductor – electrolyte surface. At the beginning the addition of glycine resulted in a drop of the potential. As can be seen, there is a point of change, after which the addition of glycine lead to the increase of the OCP. This change occurred at approximately  $9 \cdot 10^{-5} \text{ mol L}^{-1}$  and it is attributed to the concentration changes of the interacting species (electrolyte) on the surface of ZnO. This point stands for a local equilibrium between all interacting species. The concentration and OCP dependence on time for glutamic acid (pI = 3.15) is shown in Fig. 7b. Similarly, as for glycine even small changes between the standard  $0.1 \text{ mol L}^{-1} \text{ Na}_2\text{SO}_4$  solution and the  $2.44 \cdot 10^{-5} \text{ mol L}^{-1}$  solution of glutamic acid leads to different OCP time evolution. For the glutamic acid an increase of the potential was observed with increasing concentration. Next additions of glutamic acid changed the charge on the surface and the OCP was of around 100 mV higher than for glycine, as can also be seen in Fig. 6b. In the case of glutamic acid, its acidic properties lead to an increase of potential up to 160 mV. The Fig. 7c represents the concentration and OCP dependence on time for histidine, a representative of alkaline structures (pI = 7.6). A totally different behavior can be seen in the concentration dependence of histidine on the OCP value evolution compared to glycine and glutamic acid. There was an instantaneous decrease of OCP after addition of first 0.5 ml solution of histidine ( $c_{\text{His}} = 2.44 \cdot 10^{-5} \text{ mol L}^{-1}$ ). However, after next additions of histidine solution almost no changes of the OCP was observed. From that results it is evident that the alkaline behaving histidine charged the layer oppositely. The direct comparison of OCP behavior of three individual aminoacids at one concentration ( $4.76 \cdot 10^{-5} \text{ mol L}^{-1}$ ) with undoped layer of ZnO is shown in Fig. 8. The aminoacids behaved very distinctly even at low concentrations. Increases of potentials were observed for acidic aminoacids and a decrease in potential for histidine. This evidently shows the dependence of the polarity of aminoacids (pI) and the basicity (alkalinity) on the OCP measurement.

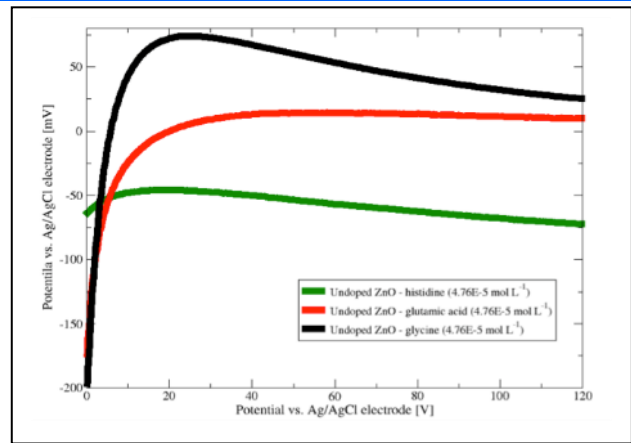
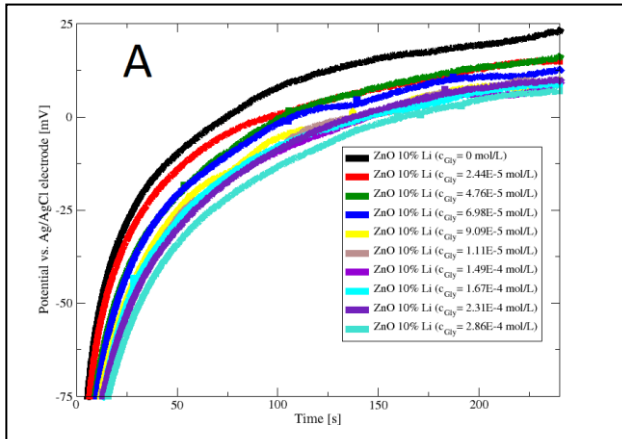


Fig. 8: Comparison of OCP measurements for three individual amino acids on undoped ZnO layer with one concentration ( $4.76 \cdot 10^{-5} \text{ mol L}^{-1}$ )

For Li and Na doped layers an increased selectivity against the aminoacids was sought. It should also be noted that the steadiness of the OCP signal (Fig. 9) was low for all measurements with 10 mol. % Li doped layers. The Fig. 9a represents the concentration and OCP on time dependence for glycine and 10 mol. % Li doped layers of ZnO. The Fig. 9b represents the concentration and OCP on time dependence for glycine measured with 10 mol. % Na doped layers of ZnO, where, at higher starting potential (0 mV), it was seen its role on the stability of the OCP signal over time. This shift changed only the initial charge deposited at the ZnO - electrolyte interface, but not the general trend. As can also be seen in Fig. 9b, the modification of the starting potential change had almost no effect on the OCP dependence trend on concentration. The increasing concentration of glycine leads to decrease of the OCP in the whole range of potentials for thin layers of ZnO with 10 mol. % Li in comparison with the undoped layers (Fig. 6a) and 10 mol. % Na (Fig. 9b). These results showed the important role of polarity change caused by doping, on the OCP response to the glycine. From Figs. 9a and 9b it can be concluded, that the role of doping by 10 mol. % Li and 10 mol. % Na lead to opposite response of glycine to the layer. This trend indicates another binding mechanism of aminoacid on the ZnO layer. This stands for the electrical charging-up of the ZnO-amino acid solution interface at constant the pH value of the electrolyte (pH 6). To validate results obtained for simple oxygen containing aminoacids also for more complex aminoacids with sulphur the OCP measurements for all type of layers were also performed with methionine at two concentrations. As can be clearly seen in Fig. 10 the course of the potential curve in time for the methionine strongly depends on the polarity of prepared layers similarly to the other aminoacids. The dopation of 10 mol. % Na resulted in a minor, but an evident change of OCP behavior. This difference of the OCP behavior is even more clearly seen for 10 mol. % Li doped layers. A very small change of methionine concentration had a substantial effect on the interfacial kinetics between the layers and the solution. For undoped layers the change

Fig. 9a: OCP measurement with glycine on ZnO layer doped with 10 mol. % Li



is clearly evident in the first 60 s, after which the difference became small. The initial disturbance of the system allowed determining the response of the aminoacid on the interactions occurring on the ZnO layers. From Figs. 9 and 10 it can be concluded that the structure of aminoacids together with their polarities plays the most crucial role on their electrochemical properties. A very diverse behavior under OCP measurement was seen for acidic (glutamic acid) (Fig. 7a) and alkaline (histidine) aminoacids for undoped layers (Fig. 7c). The Fig. 10 also shows that this system using doped layers of ZnO and individual aminoacid permits both quantitative and qualitative description of aminoacids behavior in the sense of OCP measurement.

#### IV. CONCLUSIONS

Three types of ZnO layers on ITO glass substrate were successfully prepared by sol-gel method. It was shown that the doping of ZnO layers by 10 mol. % Li and 10 mol. % Na had nearly no effect on the crystalline size and structural properties, however, the change of the electrochemical properties caused by doping was really significant. It was found that the photo-electrochemical properties of ZnO layers by means of amperometry were enhanced dramatically by doping.

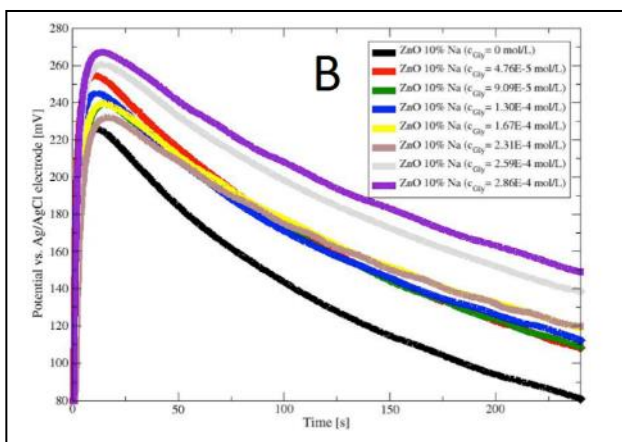


Fig. 9b: OCP measurement with glycine on doped with 10 mol. % Na

Nevertheless, the stability of 10 mol. % Li doped ZnO layers was low which was confirmed by second run amperometry. This was in contradiction to 10 mol. % Na doped and undoped ZnO layers.

A series of OCP measurements, which were performed for undoped layers of ZnO with the electrolyte in which aminoacids were dissociated, shown a strong but very distinct interaction of all aminoacids to the ZnO surface. The strength of the interaction was directly reflecting the polarity and size of the aminoacids molecule. The glycine and glutamic acid revealed a similar interaction at higher concentrations. For glycine the small addition resulted in a significant drop of the OCP, meanwhile for glutamic acid the OCP increased with concentration. There is a point of change for glycine at approximately  $9 \cdot 10^{-5} \text{ mol L}^{-1}$ , which stands for a local equilibrium between all interacting species after which their addition lead to the increase of the OCP. Histidine molecules interacted oppositely. There was an instantaneous decrease of OCP after small addition of histidine, which stop at  $4.76 \cdot 10^{-5} \text{ mol L}^{-1}$  and next additions of histidine had no effect on the OCP.

A similar series of measurements done for 10 mol. % Na and 10 mol. % Li doped layers confirmed that the change of ZnO polarity caused by doping played a very important role in the OCP detection of aminoacids. The OCP signal was low for all measurements with 10 mol. % Li doped layers, whereas, the OCP signal was significantly higher with 10 mol. % doped Na layers of ZnO. A strong dependence on layer polarity was also confirmed for methionine; sulphur contained aminoacid. The layers doped with 10 mol. % Li were the most active while 10 mol. % Na doped and undoped layers were not selective. It was proved that the systematic OCP approach to the electrolyte containing aminoacids allowed the qualitative distinction among four types of aminoacids and also the quantitative analysis, when only one aminoacid was presented in the electrolyte.

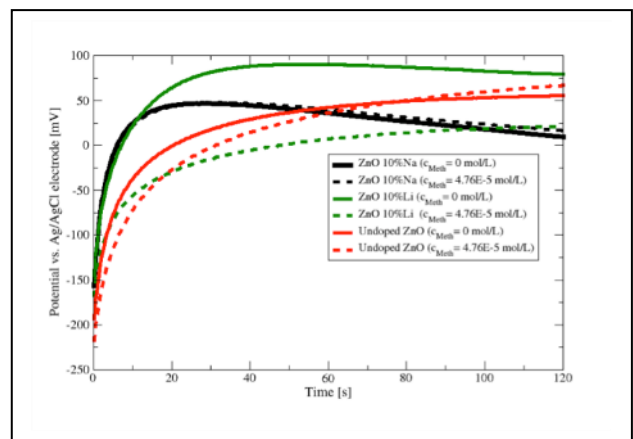


Fig. 10: Comparison of undoped and doped ZnO layers response to methionine in OCP measurement

#### ACKNOWLEDGMENT

The support of Grant Agency of the Czech Republic (grant No. 15-14228S) and (grant No. 15-04790S) are gratefully acknowledged.

## REFERENCES

- [1] Ü. Özgür, Ya.I. Alivov, C. Liu, A. Teke, M.A. Reshchikov, S. Doğan, V. Avrutin, S.-J. Cho, A. Morkoç, A comprehensive review of ZnO materials and devices, *J. Appl. Phys.* 98 (2005) 103-131.
- [2] J.E. Jaffe, A.C. Hess, Hartree-Fock study of phase changes in ZnO at high pressure, *Phys. Rev. B* 248 (1993) 7903-7909.
- [3] W.M. Haynes (Ed.), *CRC Handbook of Chemistry and Physics*, 95th Ed, CRC Press, Boca Raton, FL, 2014, Section 12 (90).
- [4] J.F. Muth, R.M. Kolbas, A.K. Sharma, S. Oktyabrsky, J. Narayan, Excitonic structure and absorption coefficient measurements of ZnO single crystal epitaxial films deposited by pulsed laser deposition, *Appl. Phys.* 85 (1999) 7884-7887.
- [5] K. Thonke, T. Gruber, N. Teofilov, R. Schönfelder, A. Waag, R. Sauer, Donor-acceptor pair transitions in ZnO substrate material, *Physica B* 308-310 (2001) 945-948.
- [6] D.C. Reynolds, D.C. Look, B. Jogai, C. W. Litton, T.C. Collins, W. Harsch, G. Cantwell, Neutral-donor-bound-exciton complexes in ZnO crystals, *Phys. Rev. B* 57 (1998) 12151-12155.
- [7] E.V. Lavrov, J. Weber, F. Börrnert, C.G. van de Walle, R. Helbig, Hydrogen-related defects in ZnO studied by infrared absorption spectroscopy, *Phys. Rev. B* 66 (2002) 165205-165507.
- [8] G. Sberveglieri, S. Gropelli, P. Nelli, A. Tintinelli, G. Giunta, A novel method for the preparation of NH<sub>3</sub> sensors based on ZnO-In thin films, *Sensors and Actuators B: Chemical* (1-3) (1995) 25, 588-590.
- [9] T. Mitsuyu, S. Ono, K. Wasa, Structures and SAW properties of rf-sputtered single-crystal films of ZnO on sapphire, *J. Appl. Phys.* 51 (1980) 2464-2470.
- [10] A. Hachigo, H. Nakahata, K. Higaki, S. Fujii, S. Shikata, Heteroepitaxial growth of ZnO films on diamond (111) plane by magnetron sputtering, *Appl. Phys. Lett.* 65 (1994) 2556-2558.
- [11] K.-K. Kim, J.-H. Song, H.-J. Jung, W.-K. Choi, S.-J. Park, J.-H. Song, The grain size effects on the photoluminescence of ZnO/ $\alpha$ -Al<sub>2</sub>O<sub>3</sub> grown by radio-frequency magnetron sputtering, *J. Appl. Phys.* 87 (2000) 3573-3575.
- [12] K.-K. Kim, J.-H. Song, H.-J. Jung, W.-K. Choi, S.-J. Park, J.-H. Song, J.-Y. Lee, Photoluminescence and heteroepitaxy of ZnO on sapphire substrate (0001) grown by rf magnetron sputtering, *J. Vac. Sci. Technol., A* 18 (2000) 2864-2868.
- [13] P. Fons, K. Iwata, S. Niki, A. Yamada, K. Matsubara, Growth of high-quality epitaxial ZnO films on  $\alpha$ -Al<sub>2</sub>O<sub>3</sub>, *J. Cryst. Growth* 201-202 (1999) 627-632.
- [14] S.K. Tiku, C.K. Lau, K.M. Lakin, Chemical vapor deposition of ZnO epitaxial films on sapphire, *Appl. Phys. Lett.* 36 (1980) 318-319.
- [15] M. Kasuga, M. Mochizuki, Orientation relationships of zinc oxide on sapphire in heteroepitaxial chemical vapor deposition, *J. Cryst. Growth* 54 (1981) 185-194.
- [16] P. Dytrych, P. Kluson, P. Dzik, M. Vesely, M. Morozova, Z. Sedlakova, O. Solcova, Photoelectrochemical properties of ZnO and TiO<sub>2</sub> layers in ionic liquids environment, *Catal. Today* 230 (2014) 152-157.
- [17] L. Spanhel, M. A. Anderson, Semiconductor clusters in the sol-gel process: quantized aggregation, gelation, and crystal growth in concentrated zinc oxide colloids, *J. Am. Chem. Soc.* 113 (1991) 2826-2833.
- [18] M. Ohyama, H. Kozuka, T. Yoko, Sol-gel preparation of ZnO films with extremely preferred orientation along (002) plane from zinc acetate solution, *Thin Solid Films* 306 (1997) 78-85.
- [19] H.B. Zheng, J.B. Cui, B.Q. Cao, U. Gibson, Y. Bando, D. Goldberg, Electrochemical deposition of ZnO nanowire arrays: organization, doping, and properties, *Sci. Adv. Mater.* 3 (2010) 336-358.
- [20] H.N. Chen, W.P. Li, Q. Hou, H.C. Liu, L.Q. Zhu, Growth of three-dimensional ZnO nanorods by electrochemical method for quantum dots-sensitized solar, *Electrochim. Acta* 24 (2011) 8358-8364.
- [21] J.H. Qiu, M. Guo, Y.J. Feng, X.D. Wang, Electrochemical deposition of branched hierarchical ZnO nanowire arrays and its photoelectrochemical properties, *Electrochim. Acta* 16 (2011) 5776-5782.
- [22] S. Golshani, S.M. Rozati, R. Martins, E. Fortunado, P-type ZnO thin film deposited by spray pyrolysis technique: The effect of solution concentration, *Thin Solid Films* 518(4) (2009) 1149-1152.
- [23] G. Nawrocki, M. Cieplak, Amino acids and proteins at ZnO-water interfaces in molecular dynamics simulations, *Phys. Chem. Chem. Phys.*, 15 (2013) 13628-13636.
- [24] N. Subramaniana, A. Al Ghaferi, An aminoacid-based swift synthesis of zinc oxide nanostructures, *RSC Adv.* 4 (2014) 4371-4378.
- [25] A. Brif, G. Ankonina, C. Drathen, B. Pokroy, Bio-Inspired Band Gap Engineering of Zinc Oxide by Intracrystalline Incorporation of Amino Acids, *Adv. Mat.* 26(3) (2014) 477-481.
- [26] J. Lee, S. Cha, J. Kim, H. Nam, S. Lee, W. Ko, K.L. Wang, J. Park, J. Hong, p-Type Conduction Characteristics of Lithium-Doped ZnO Nanowires. *Adv. Mater.*, 23 (2011) 4183-4187.
- [27] A. Saaedi, R. Yousefi, F. Jamali-Sheini, M. Cheraghizade, A.K. Zak, N.M. Huang, Optical and electrical properties of p-type Li-doped ZnO nanowires, *Superlattice. Microst.* 61, (2013) 91-96.
- [28] S.G. Pawley, Unit cell refinement from powders diffraction scans, *J. App. Cryst.*, 14(6) (1981), 357-361.
- [29] Y. J. Zeng, Z. Z. Ye, J. G. Lu, W. Z. Xu, L. P. Zhu, and B. H. Zhao, Identification of acceptor states in Li-doped p-type ZnO thin films *App. Phys. Lett.* 89 (2006) 042106.
- [30] W. Chen, X. H. Pan, S. S. Chen, H. P. He, J. Y. Huang, B. Lu, Z. Z. Ye, Investigation on non-polar m-plane ZnO and Na-doped p-type ZnO films grown by plasma-assisted molecular beam epitaxy, *App. Physics* 121 (2015) 77-82.
- [31] G.C. Barrett, D. T. Elmore, *Amino Acids and Peptides*, Cambridge University Press, Cambridge, New York, (1998), *Physicochemical properties of amino acids and peptides*, pp. 32-47. Academic, 1963, pp. 271-350.